Capillary Forces in Suspension Rheology

Erin Koos, *et al.*

Science **331**, 897 (2011);
DOI: 10.1126/science.1199243

17. Y. Lassailly, H. Drouhin, A. van der Sluijs, G. Lampel, C. Marliere, *Phys. Rev. B* **50**, 13054 (1994).
18. D. P. Pappas *et al.*, *Phys. Rev. Lett.* **66**, 504 (1991).
19. C. Gröbli, D. Guarisco, S. Frank, F. Meier, *Phys. Rev. B* **51**, 2945 (1995).
20. M. Getzlaff, J. Bansmann, G. Schönhense, *Solid State Commun.* **87**, 467 (1993).
21. C. Cacho, Y. Lassailly, H.-J. Drouhin, G. Lampel, J. Peretti, *Phys. Rev. Lett.* **88**, 066601 (2002).
22. G. Schönhense, H. C. Siegmann, *Ann. Phys. (Leipzig)* **2**, 465 (1993).
23. H. J. Drouhin, *Phys. Rev. B* **56**, 14886 (1997).
24. T. Maruyama *et al.*, *Phys. Rev. Lett.* **66**, 2376 (1991).
25. S. Mayer, J. Kessler, *Phys. Rev. Lett.* **74**, 4803 (1995).
26. S. S. Skourtis, D. N. Beratan, R. Naaman, A. Nitzan, D. H. Waldeck, *Phys. Rev. Lett.* **101**, 238103 (2008).
27. S. Yeganeh, M. A. Ratner, E. Medina, V. Mujica, *J. Chem. Phys.* **131**, 014707 (2009).
28. G. A. Prinz, *Science* **282**, 1660 (1998).
29. S. A. Wolf *et al.*, *Science* **294**, 1488 (2001).
30. D. D. Awschalom, M. E. Flatté, *Nat. Phys.* **3**, 153 (2007).

31. T.Z.M. and R.N. acknowledge the partial support from the Israel Science Foundation.

Supporting Online Material

www.sciencemag.org/cgi/content/full/331/6019/894/DC1
Materials and Methods
Figs. S1 to S8
References

20 October 2010; accepted 20 December 2010
10.1126/science.1199339

Capillary Forces in Suspension Rheology

Erin Koos* and Norbert Willenbacher

The rheology of suspensions (solid particles dispersed in a fluid) is controlled primarily through the volume fraction of solids. We show that the addition of small amounts of a secondary fluid, immiscible with the continuous phase of the suspension, causes agglomeration due to capillary forces and creates particle networks, dramatically altering the bulk rheological behavior from predominantly viscous or weakly elastic to highly elastic or gel-like. This universal phenomenon is observed for a rich variety of particle/liquid systems, independent of whether the second liquid wets the particles better or worse than the primary liquid. These admixtures form stable suspensions where settling would otherwise occur and may serve as a precursor for microporous polymer foams, or lightweight ceramics.

The rheology and flow of suspensions is usually controlled by the interplay between the attractive van der Waals forces, repulsive electrostatic forces, or steric interactions among particles hydrodynamic interactions and Brownian forces (*1*–*6*). Capillary forces, which play a dominant role in wet granular materials, can also be an important factor in suspensions. In granular media, the addition of water, either directly or due to aging in a humid environment (*7*, *8*), is associated with an increase in the angle of repose and grain cohesiveness (*9*–*11*). The water wets the grains, creating a network of grains connected by pendular bridges, and allows, for example, the creation of complex structures such as sandcastles (*12*, *13*). In suspensions, this behavior can be reproduced through the addition of small amounts of a second immiscible fluid that preferentially wets the solid particles (*14*–*16*) and creates pendular bridges between particles causing the agglomeration of individual particles and, if the volume fraction of solids is sufficient, creates a network of particles within the bulk fluid. The addition of this secondary "binder" fluid will cause an increase in sedimentation volume (*17*–*19*), indicating network formation within the suspension. This agglomeration of particles has been used to separate solids from bulk fluid (*20*) in coal and ore preparation (*21*, *22*), to separate oil sands, and for dye-pigment preparation (*23*). This state, in which the secondary fluid preferentially wets the particles, is termed the "pendular" state because of the pendular bridges formed between particles. This state is analogous to the pendular state in wet granular media in which the fluid saturation is small and is primarily responsible for the granulation of powders (*24*, *25*).

In addition to particle agglomeration caused by the addition of a binder fluid in the pendular state, one can imagine a situation where the second immiscible fluid does not preferentially wet the particles. In this state, though the second fluid is attached to the particles and agglomeration still occurs, there is no pendular bridge formed between the particles. The addition of the secondary fluid is able to agglomerate the particles and create sample-spanning network structures due to the strong capillary force from the bulk wetting fluid. This state is analogous to the capillary state in wet granular media, where almost all of the pores between particles are filled with water (or another wetting fluid) (*26*, *27*). In wet granular materials, strong cohesive strength is observed slightly below complete saturation of the solids by the wetting fluid. In these suspensions, the secondary, preferentially nonwetting fluid is playing the part of the unfilled voids in wet granular materials where the saturation by the preferentially wetting fluid is high. In our analogy to wet granular materials, we term these admixtures "capillary" suspensions.

Despite how well the analogy describes the behavior—and the use of capillary forces in suspensions for solid/liquid separation for more than a century (*20*)—this phenomenon has not been considered with respect to rheology and formulation of stable suspensions at particle loadings substantially lower than dense pack-

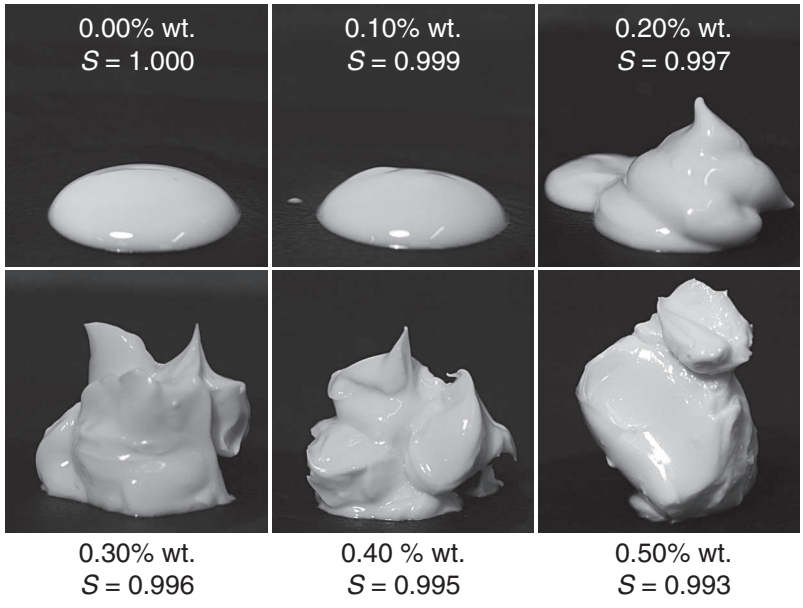

Fig. 1. The transition from weakly elastic, fluidlike behavior to highly elastic, gel-like behavior is visible with the addition of small amounts of water to a suspension of hydrophobically modified calcium carbonate (Socal, $r = 0.8$ μm, $\phi = 0.111$) in DINP. The wetting angle between the solid and water in DINP is $\theta = 139.2°$, and S is the percentage of the total liquid volume occupied by preferentially wetting fluid DINP (*31*).

Institute for Mechanical Process Engineering and Mechanics, Karlsruhe Institute of Technology, Gotthard-Franz-Straße 3, Building 50.31, 76131 Karlsruhe, Germany.

*To whom correspondence should be addressed. E-mail: erin.koos@kit.edu

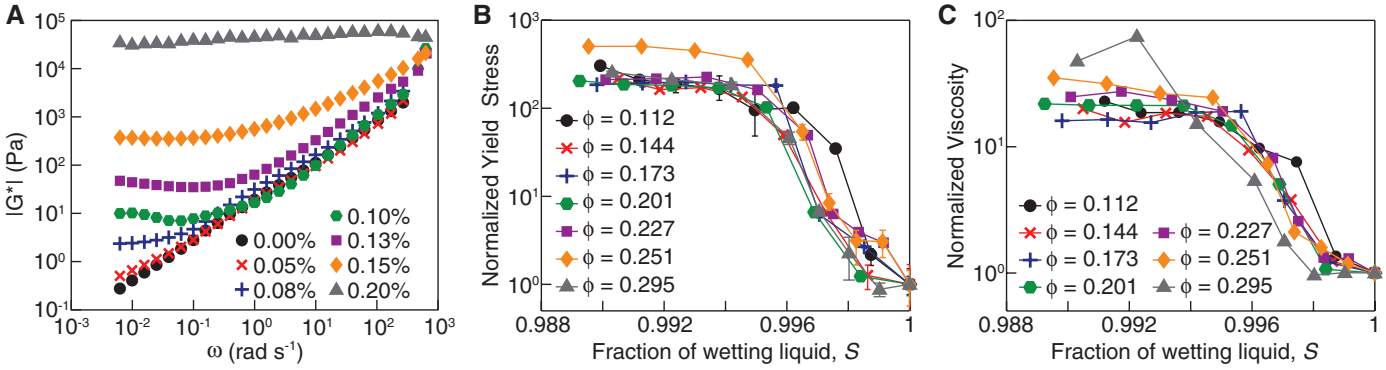

Fig. 2. Effect of added water on an oil-based suspension (capillary state). (**A**) Magnitude of the complex shear modulus for Socal in silicone oil (AK1000, ϕ = 0.173) for varying weight percentages of water showing the transition from fluidlike to highly elastic, gel-like behavior. |G*|, magnitude of the complex shear modulus; ω, angular frequency; rad, radians. (**B**) Normalized yield stress and (**C**) normalized viscosity at a single shear rate of $\dot{\gamma} = 1\ s^{-1}$, for various volume fractions of Socal in DINP. The yield stress in (B) and viscosity in (C) are normalized by the value at $S = 1$, where only DINP is present. The wetting angles for the water are $\theta = 122.8°$ (A) and $\theta = 139.2°$ [(B) and (C)]; see table S1. Error bars in (B) indicate repeatability error.

ing. Such capillary suspensions, which include a small fraction of a preferentially nonwetting fluid, have recently been investigated because of their influence on the aging of polyvinyl chloride (PVC) plastisol mixtures [PVC particles suspended in a plasticizer such as diisononyl phthalate (DINP)] caused by the uptake of water (*28*–*30*), but without a clear understanding that capillary forces were the cause of the observed transition. These capillary suspensions are quite sensitive to the addition of the secondary fluid, as seen in Fig. 1 and movie S1. The transition from a fluidlike state to a gel-like state occurs with as little as 0.2 weight percent (wt %) of the second fluid in suspensions with a volume of solids ϕ as low as 10%.

We took measurements with the use of several different fluid/particle combinations with particles of a wide variety of sizes and shapes, as shown in fig. S1 and described in table S1 (*31*). We measured contact angles for each fluid in air and then used the results to calculate the contact angle that the secondary fluid makes against the solid particles in the bulk fluid environment using surface energy components (*31*–*33*). These contact angles fall into two groups: (i) those smaller than 90°, where the mixture is in the pendular state, and (ii) those greater than 90°, where the mixture is in the capillary state.

In the capillary state, we used the hydrophobically modified calcium carbonate (Socal, Solvay Advanced Functional Minerals, Salin de Giraud, France) in DINP or silicone oil as a model system. The transition between the weakly elastic, fluidlike behavior to highly elastic, gel-like behavior can be observed through measurements of the shear modulus conducted using a small-amplitude oscillatory shear (Fig. 2A). Without added water, the magnitude of the complex shear modulus increases linearly with increasing frequency, but as small weight percentages of water are added to the suspension of Socal in silicone oil, the shear modulus begins to increase at low frequencies. At 0.20 wt % of added water, the mixture becomes highly elastic, and the complex shear modulus is nearly constant with frequency.

We varied the amount of water (the secondary fluid) between 0.0 and 0.8% by mass, corresponding to a saturation S of the wetting fluid between 1.00 and 0.99. Each mixture was characterized in steady shear by measuring the yield stress (*31*) and steady-state viscosity, as shown in Fig. 2, B and C, respectively. In Fig. 2B, the yield stress when water was present, normalized against the yield stress measured when no water is present ($S = 1$), is displayed as a function of the wetting-liquid fraction. These mixtures are very sensitive to the addition of water, increasing the yield stress by more than two orders of magnitude over the single-fluid suspensions. This increase in the normalized yield stress is independent of the volume fraction of solids. Each volume-fraction experiment shows a characteristic curve with the most rapid change in yield stress occurring at a fraction of 0.997. Below a wetting fluid fraction of 0.995, the curves plateau.

As with the yield stress, the viscosity (Fig. 2C) evaluated at a single shear rate ($\dot{\gamma} = 1\ s^{-1}$) also increases by more than one order of magnitude from the $S = 1$ value. The transition from the low-viscosity, fluidlike behavior to the high-viscosity, gel-like behavior occurs at a saturation of the wetting fluid of 0.997. This transition in viscosity occurs at the same saturation point as the yield stress shows a dramatic increase. Furthermore, the viscosity measurements show the same coincidence of the curves with varying volume fraction. This change in the normalized viscosity is only slightly more than one order of magnitude, so it is less pronounced than the increase in the normalized yield stress.

The gel-like transition in capillary suspensions dramatically increases the yield stress and viscosity above the corresponding values from the single-fluid suspensions. The full dependence of yield stress on the saturation, the fraction of available volume filled by the wetting fluid, is shown in Fig. 3 for PVC (C12/62V, Vinnolit, Ismaning, Germany) and hematite, both in various percentages of water and DINP. For the PVC system, the yield stress increases slightly in the pendular state (where DINP is the primary fluid) and increases greatly in the capillary state (where water is the primary fluid). The greatest increase in the yield stress occurs at a saturation of $S = 0.7$, in the capillary state, for the PVC as well as many of the other liquid/particle combinations that we tested (for example, Socal and hydrophobic glass). For hematite and similar systems (for instance, silica and hydrophilic glass), the transition in the pendular state is more pronounced

Fig. 3. Dependence of the yield stress on the fraction of the wetting liquid. For this PVC (Vinnolit C12/62V), the increase in yield stress is greatest in the capillary state, in which water is the primary fluid and DINP is the secondary fluid. For the hematite, the increase in yield stress is greatest in the pendular state, in which DINP is the primary fluid and water is the secondary fluid. The saturation is defined as the fraction of total fluid volume occupied by the preferentially wetting fluid. Error bars indicate repeatability error.

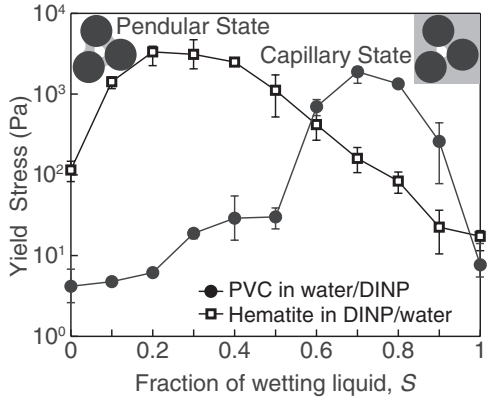

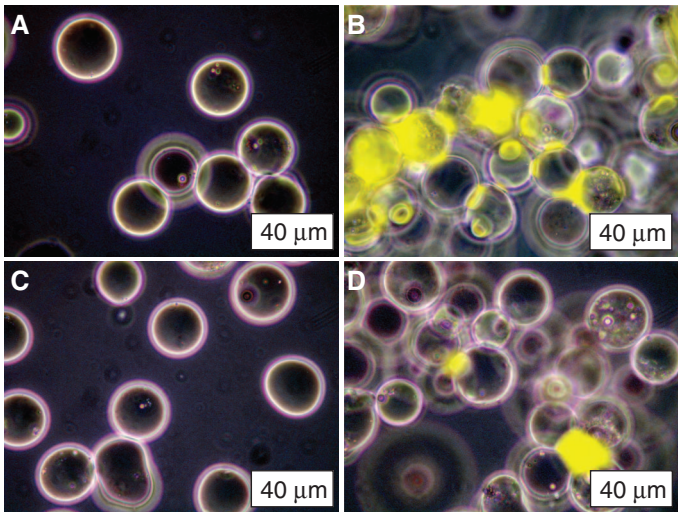

Fig. 4. Images of the pendular and capillary states. Clean glass (hydrophilic, θ = 49.4°, r = 12.3 μm, ϕ = 0.3; see table S1) in DINP with (**A**) no added water and (**B**) with 1 wt % added water. Treated glass (hydrophobic, θ = 99.3°) in DINP with (**C**) no added water and (**D**) 1 wt % added water. The composite images with added water [(B) and (D)] in the pendular and capillary states, respectively, are composed of the fluorescent dye image in yellow, used to highlight the secondary fluid, merged onto the corresponding real light image (see fig. S4).

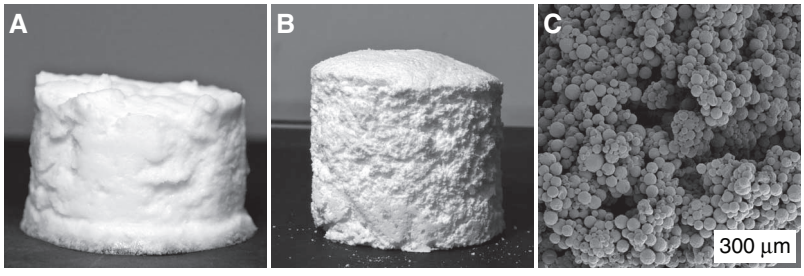

Fig. 5. PVC foam and solid. Mixture of PVC in water with added DINP (ϕ = 0.20, S = 0.973) shown (**A**) without any treatment and (**B**) after the water is removed under vacuum (100 mbar for 24 hours) with additional heating (70°C for 6 hours). (**C**) Micrograph of the heated (fused) foam.

with the highest yield stresses observed for low-saturation values around S = 0.2.

Particles can create stable flocculated networks in suspensions through the effects of the van der Waals forces; they are much smaller than the capillary force between particles considered here (*34*). Typical values of the force due to a capillary bridge between two particles in contact (F_c) are given by

$$F_c = 2\pi r\Gamma\cos\theta \approx 300 \text{ nN} \quad (1)$$

where the particle radius r is 10^{-6} m, the surface tension Γ is 50×10^{-3} N·m^{-1}, and the wetting angle θ is small ($\cos\theta \approx 1$). The typical value for the van der Waals force (F_{vdW}) is much smaller

$$F_{vdW} = \frac{A_H}{12}\frac{r}{h^2} \approx 1 \text{ nN} \quad (2)$$

where the particle separation is given by the surface roughness $h = 10^{-9}$ m and Hamaker's coefficient A_H has a value of 10^{-20} N·m. The capillary force serves as the dominant factor influencing the agglomeration of particles. Although the magnitude of the capillary force may be reduced (e.g., due to particle separation, variations in wetting angles, or small pendular bridge volume), capillary forces due to a second immiscible fluid have a great potential for increasing or strengthening the particle network formation within suspensions.

There are other factors that may cause the agglomeration of particles and the observed increase in gel strength. One such factor is the displaced volume caused by the addition of the second immiscible fluid. The effective volume fraction for solid particles and drops of the secondary fluid contained within the bulk fluid may approach the random close-packing volume fraction, causing a substantial rise in the viscosity. This explanation, however, does not account for the transition observed at low-volume fractions (as low as ϕ = 0.1 for the DINP-calcium carbonate mixtures). The very small addition (0.2 wt %) of a secondary fluid does not increase the volume fraction of the dispersed phase significantly.

Cavalier and Larché suggested that hydrogen bonds between water molecules might explain the transition in which water is the secondary fluid (as it was in their dioctyl phthalate–calcium carbonate mixtures) (*30*). However, we observe a similar capillary-state transition using PVC particles suspended in water with added DINP. In this case, the lack of any available H-bonding protons in the molecule makes hydrogen bonding an unlikely mechanism for the transition.

We used a microscope to image suspensions of glass beads with hydrophilic and hydrophobic surface treatments in DINP with and without the addition of water as a secondary fluid (*31*). We used a fluorescent dye to mark the location of the water in these images, which are shown in Fig. 4B for the pendular state and Fig. 4D for the capillary state. Corresponding images of the suspensions without the addition of a secondary fluid are shown in Fig. 4, A and C. In the pendular state, the water preferentially wets the glass beads, and the circular outlines of capillary bridges are clearly visible joining several of these particles tightly together. In the capillary state, the water does not preferentially wet the treated glass. In this state, the water is present as globular drops in the center of the glass agglomerates.

We investigated the effects of a second immiscible fluid on the flow of particle suspensions. We find that the addition of this second fluid can dramatically change the rheological properties of the mixture; the second fluid creates a network of interconnected particles leading to a transition to a highly elastic, gel-like state. Most notably, this effect exists—and is quite strong—even when the second fluid wets the particles less well than the primary fluid.

The addition of a second immiscible fluid has several different effects, all of which are important in industrial applications. For suspensions where settling would occur, the addition of a second fluid allows for the creation of extremely stable suspensions (as shown in movie S2) through the creation of a sample-spanning network structure. For example, both the PVC and glass particles would settle to the bottom of a container in a single-fluid suspension within a few hours, but with the addition of a secondary fluid, suspensions become so stable that they do not phase-separate when left for many weeks. This effect can be used to keep mixtures homogeneous as they are stored and transported. We also show that this process can dramatically change the yield stress and viscosity of a suspension, allowing for the creation of fluids with tunable flow or processing behavior that may be adjusted by temperature (see supporting online material) or the addition of surfactants. Most importantly, this effect is completely reversible and allows for the yield stress or viscosity to be varied to meet the needs of each step in an industrial process. Finally, the addition of a second immiscible fluid creates a strong network of particles at lower volume fractions than could be obtained otherwise. This particle network may be used as a precursor for porous ceramics or foams, such as that shown in Fig. 5. The PVC solid, which consists of only fused PVC particles, has a bulk density of 0.4 g·ml^{-1}, indicating that some compaction has occurred so that the actual volume fraction of solids is ϕ = 0.3 compared with the starting volume fraction of ϕ = 0.2. Without the secondary fluid (DINP), the creation of these light foams would be impossible, as the PVC particles would settle in the water to a much larger volume fraction, near the maximum random-packed volume fraction of ϕ = 0.6. The creation of these foams opens up a new route to material

design, aiming at lightweight construction materials, catalyst carriers with a large inner surface, or microporous foams with superior insulation properties.

References and Notes

1. C. Allain, M. Cloitre, M. Wafra, *Phys. Rev. Lett.* **74**, 1478 (1995).
2. R. Buscall *et al.*, *J. Non-Newt. Fluid Mech.* **24**, 183 (1987).
3. S. C. Tsai, K. Zammouri, *J. Rheol.* **32**, 737 (1988).
4. M. Dijkstra, *Curr. Opin. Colloid Interface Sci.* **6**, 372 (2001).
5. Z. Zhou, P. J. Scales, D. V. Boger, *Chem. Eng. Sci.* **56**, 2901 (2001).
6. P. J. Lu *et al.*, *Nature* **453**, 499 (2008).
7. L. Bocquet, E. Charlaix, S. Ciliberto, J. Crassous, *Nature* **396**, 735 (1998).
8. N. Fraysse, H. Thomé, L. Petit, *Eur. Phys. J. B* **11**, 615 (1999).
9. T. C. Halsey, A. J. Levine, *Phys. Rev. Lett.* **80**, 3141 (1998).
10. T. G. Mason, A. J. Levine, D. Ertaş, T. C. Halsey, *Phys. Rev. E* **60**, R5044 (1999).
11. G. D'Anna, *Phys. Rev. E* **62**, 982 (2000).
12. S. Herminghaus, *Adv. Phys.* **54**, 221 (2005).
13. N. Mitarai, F. Nori, *Adv. Phys.* **55**, 1 (2006).
14. H. R. Kruyt, F. G. Van Selms, *Recl. Trav. Chim. Pays-Bas* **62**, 415 (1943).
15. A. E. J. Eggleton, I. E. Puddington, *Can. J. Chem.* **32**, 86 (1954).
16. S. Van Kao, L. E. Nielsen, C. T. Hill, *J. Colloid Interface Sci.* **53**, 367 (1975).
17. W. Ostwald, W. Haller, *Kolloid (Beih.)* **29**, 354 (1929).
18. C. R. Bloomquist, R. S. Shutt, *Ind. Eng. Chem.* **32**, 827 (1940).
19. P. G. Howe, D. P. Benton, I. E. Puddington, *Can. J. Chem.* **33**, 1189 (1955).
20. A. E. Cattermole, "Classification of the metallic constituents of ores," U.S. Patent 763259 (1904).
21. G. J. Perrot, S. P. Kinney, *Chem. Metall. Eng.* **25**, 182 (1921).
22. J. R. Farnand, I. E. Puddington, *Can. Min. Metall. Bull.* **62**, 267 (1969).
23. T. Langstroth, in *Pigment Handbook*, P. A. Lewis, Ed. (Wiley, New York, 1988), vol. 3, chap. 6.
24. B. J. Ennis, J. Li, G. I. Tardos, R. Pfeffer, *Chem. Eng. Sci.* **45**, 3071 (1990).
25. B. J. Ennis, G. I. Tardos, R. Pfeffer, *Powder Technol.* **65**, 257 (1991).
26. W. Pietsch, H. Rumpf, *Chem. Ing. Tech.* **39**, 885 (1967).
27. H. Schubert, *Kapillarität in Porösen Feststoffsystemen* (Springer, Berlin, 1982).
28. B. Hochstein, N. Willenbacher, *AIP Conf. Proc.* **1027**, 761 (2008).
29. L. Tanzil, B. Hochstein, N. Willenbacher, in *Produktgestaltung in der Partikeltechnologie*, U. Teipel, Ed. (Fraunhofer Institut für Chemische Technologie, Pfinztal, Germany, 2008), vol. 4, pp. 67–75.
30. K. Cavalier, F. Larche, *Colloids Surf. A Physicochem. Eng. Asp.* **197**, 173 (2002).
31. Materials and methods are available as supporting material on *Science* Online.
32. R. Aveyard, B. P. Binks, J. H. Clint, *Adv. Colloid Interface Sci.* **100-102**, 503 (2003).
33. B. P. Binks, J. H. Clint, *Langmuir* **18**, 1270 (2002).
34. J. P. K. Seville, C. D. Willett, P. C. Knight, *Powder Technol.* **113**, 261 (2000).

35. We thank H. J. Butt for discussions and the German Research Foundation (Deutsche Forschungsgemeinschaft grant no. WI3138/6-1) for funding. We would also like to acknowledge the generous donation of materials we received from Henkel and Potters Europe.

Supporting Online Material

www.sciencemag.org/cgi/content/full/331/6019/897/DC1
Materials and Methods
SOM Text
Figs. S1 to S4
Table S1
References
Movies S1 and S2

18 October 2010; accepted 6 January 2011
10.1126/science.1199243

Steric Control of the Reaction of CH Stretch–Excited CHD_3 with Chlorine Atom

Fengyan Wang,[1] Jui-San Lin,[1] Kopin Liu[1,2]*

Exciting the CH-stretching mode of CHD_3 (where D is deuterium) is known to promote the C-H bond's reactivity toward chlorine (Cl) atom. Conventional wisdom ascribes the vibrational-rate enhancement to a widening of the cone of acceptance (i.e., the collective Cl approach trajectories that lead to reaction). A previous study of this reaction indicated an intriguing alignment effect by infrared laser–excited reagents, which on intuitive grounds is not fully compatible with the above interpretation. We report here an in-depth experimental study of reagent alignment effects in this reaction. Pronounced impacts are evident not only in total reactivity but also in product state and angular distributions. By contrasting the data with previously reported stereodynamics in reactions of unpolarized, excited CHD_3 with fluorine (F) and $O(^3P)$, we elucidate the decisive role of long-range anisotropic interactions in steric control of this chemical reaction.

The directional nature of chemical bonds generally renders intermolecular interactions and the Born-Oppenheimer potential energy surfaces (PESs) that describe such interactions anisotropic. In the course of reactions that form and break those bonds such anisotropy will tend to dynamically steer the scattering trajectories either toward or away from the transition state (a critical configuration along the reaction path, serving as a bottleneck to reaction), thereby promoting or suppressing reactivity. This steering or reorientation effect has long been recognized by chemists, and mechanistic insights at the molecular level have been garnered for a number of elementary reactions (*1*–*8*). Particularly relevant to this work are two recent studies on the reactions of CH stretch–excited, unpolarized CHD_3 ($v_1 = 1$) with F atom (*9*) and O atom (*10*).

The reaction of F + CHD_3 is highly exothermic (change in enthalpy $\Delta H_0 = -31.3$ kcal/mol) with a small early barrier, for which the transition-state structure is reactant-like. Our group found that one quantum excitation of the CH stretch ($v_1 = 1$) in CHD_3 inhibits C-H bond cleavage, resulting in a deceleration of the overall reaction rate (*9*). This unexpected finding was conjectured, and later calculated theoretically (*11*), to be a result of steering or deflection of the approaching F atom away from the targeted H atom. By contrast, an opposite effect was discovered in the O + CHD_3 reaction (*10*), which is slightly endothermic ($\Delta H_0 =$ 2.1 kcal/mol) with a barrier height of ~9.6 kcal/mol. The location of the barrier is nearly at the midpoint of the pathway; namely, the transition-state structure is neither reactant-like nor product-like. CH-stretching excitation led to a substantial rate promotion at fixed collision energy (E_c). Moreover, the product angular distribution broadened markedly from backward peaking to sideways dominant, suggesting that the vibrational enhancement operates by extending the range of impact parameters, thus opening up the cone of acceptance to reaction; this mechanism has been theoretically predicted to be particularly prominent in thermoneutral atom + diatom reactions (*6*). The driving force behind this vibrationally induced steric mechanism was further attributed to long-range anisotropic interactions, which pull or focus the trajectories toward the transition state (*10*, *12*).

A deeper implication of these two studies is that in a reaction with strong anisotropic inter-

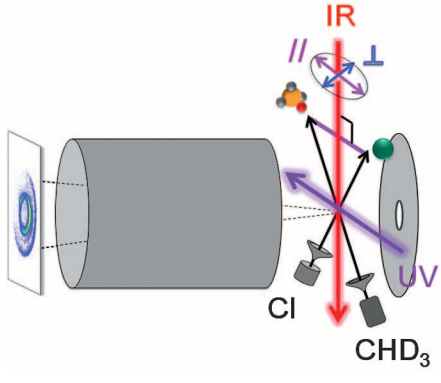

Fig. 1. Experimental setup for state-selected, aligned molecular beam scattering experiments. A linearly polarized IR laser directed perpendicularly to the relative velocity vector of the two molecular beams prepares the vibrationally excited CHD_3 at the scattering center. Reagent alignment is controlled by IR laser polarization direction: "//" refers to an end-on attack and "⊥" to a side-on approach. Time-sliced velocity-map imaging reveals the alignment effects on product pair–correlated distributions.

[1]Institute of Atomic and Molecular Sciences (IAMS), Academia Sinica, Taipei, Taiwan 10617. [2]Department of Physics, National Taiwan University, Taipei, Taiwan 10617 and Department of Chemistry, National Tsing Hua University, Hsinchu, Taiwan 300.

*To whom correspondence should be addressed. E-mail: kliu@po.iams.sinica.edu.tw